Velocity of Large Drops and Bubbles in Media of Infinite or Restricted Extent

TIBOR Z. HARMATHY

National Research Council of Canada, Ottawa, Canada

A new theory gives a simple method of calculating the terminal velocity of fluid particles moving in media of either infinite or restricted extent.

Empirical and semiempirical formulas [Equations (27) and (30)] and a graph (Figure 6) over the interval $0 \leq d/D \leq 1.3$ are shown to yield satisfactory results for gas or liquid particles moving in liquid media. In the case of liquid drops falling through gaseous media they give only a rough approximation.

Graphs showing the variation of the drag coefficient (Figure 1) and the shape (Figure 2) of fluid particles with the Eötvös number are given. A semiempirical equation for the terminal velocity of solid spheres in restricted media has also been developed [Equation (24)].

The necessity of studying the motion of large drops and bubbles in media of restricted extent has arisen in connection with an investigation into the throughput characteristics of packed liquid-extraction towers. Since the subject has been inspired by a special problem of liquid extraction, the liquid-liquid systems receive principal attention; however efforts have been made to develop a generalized theory of the behavior of drops and bubbles.

This paper deals only with drops and bubbles for which the Reynolds number is larger than 500. In practice these large drops and bubbles are by far the most interesting. The region of $N_{Re} > 500$ is characterized as the one in which the viscous effects are negligible. The shape of the fluid particles may be oblate ellipsoidal (regular or irregular), spherical cap, or cylindrical.

In the past decade several papers have been concerned with the motion of ellipsoidal drops in liquid media of practically infinite extent (*12, 23, 25, 26, 27, 31, 50*). A few other papers have dealt with the movement of drops in liquid media of more definitely restricted extent (*46, 47, 48*). To the writer's knowledge no attention has so far been paid to the motion of cylindrical drops.

The problem of velocity and behavior of liquid drops in gas has also attracted considerable interest (*2, 15, 24, 29*). These papers deal only with droplets moving or suspended in media of practically unlimited extent.

The most elaborate part of the hydrodynamics of fluid particles is that concerned with the motion of gas bubbles in liquids. An excellent review of the papers published before 1953 on this subject can be found in a report by Haberman and Morton (*16*). Since that time the motion of ellipsoidal (*36, 42, 45*), spherical cap-shaped (*36, 45*), and cylindrical (*28*) bubbles was further studied, and also the effect of wall proximity on the rise of bubbles (*49*).

From these papers and other sources it is learned that the small fluid particles are of spherical or slightly ellipsoidal shape and move in rectilinear paths. The larger ones assume a more definite ellipsoidal shape, becoming more and more distorted and less definite with increasing size, and move along zigzag or helical paths, the amplitude of which decreases with increasing deformation. The quite large fluid particles have a spherical cap shape, and their motion is practically rectilinear. The proximity of the channel wall reduces the velocity to an extent which is primarily a function of the size of the particle and of the channel (which is generally a circular tube). If the fluid particle is larger than the tube, it assumes a cylindrical shape, and its velocity depends mainly on the tube diameter.

Observations show that the oscillating motion of fluid particles moving in a relatively unrestricted medium appears around $N_{Re} = 500$; thus the appearance of the zigzagging or spiralling can be regarded as the beginning of the region of turbulent flow conditions, in which the author's correlations are applicable.

VELOCITY IN INFINITE MEDIA

It is a well-known fact that under turbulent flow conditions the drag coefficient of particles of identical shape is over a wide range practically independent of the Reynolds number. In the case of fluid particles this fact is however not immediately obvious. Several reports have been published (*16, 23, 25, 27, 31, 36, 40*) which seem to show that the drag coefficient is strongly dependent upon the Reynolds number, but this apparent contradiction vanishes if one considers that for fluid particles the variation of the Reynolds number is generally accompanied by variation of the particle shape and that the drag coefficient does depend on the shape of the object. It is therefore the shape of the fluid particle, not the Reynolds number, that is responsible for the variation of the drag coefficient in the region of turbulent flow.

The drag coefficient is generally defined by

$$C = \frac{F}{\frac{1}{2}\rho_c u^2 A} \qquad (1)$$

However when one is dealing with the motion of fluid particles, it is more convenient to regard the equivalent diameter of the particle as the characteristic length and to define a new drag coefficient with the following equation:

$$C^* = \frac{F}{\frac{1}{2}\rho_c u^2 \frac{d^2\pi}{4}} \qquad (2)$$

If a β factor defined as

$$\beta = \sqrt{\frac{A}{\frac{d^2\pi}{4}}} \qquad (3)$$

is introduced, then the correlation between the two kinds of drag coefficients becomes

$$C^* = \beta^2 C \qquad (4)$$

From geometric correlations the following expressions can be obtained:

for oblate spheroids

$$\beta = \sqrt[3]{\frac{a}{b}} \qquad (5)$$

for spherical caps

$$\beta = \frac{\frac{a}{b}}{\sqrt[3]{1 + \frac{3}{4}\left(\frac{a}{b}\right)^2}} \qquad (6)$$

If the particle is moving with its

terminal velocity, $F = (d^3\pi/6)\Delta\rho g$. A substitution into Equation (2) thus gives an expression for the terminal velocity:

$$u = K\sqrt{\frac{g\Delta\rho d}{\rho_o}} \qquad (7)$$

where

$$K = \sqrt{\frac{4}{3C^*}} \qquad (8)$$

or

$$K = \frac{1}{\beta}\sqrt{\frac{4}{3C}} \qquad (9)$$

For spheres $\beta = 1$, and in infinite media $C_{s\infty} = 0.44$ and $K_{s\infty} = 1.74$, as is well known from various handbooks.

For the time being only the terminal velocity of the particles in infinite media will be considered. From Equations (7), (8), and (9) the following correlations can be obtained:

$$\frac{u_\infty}{u_{s\infty}} = \sqrt{\frac{C_{s\infty}}{C^*_\infty}} \qquad (10)$$

or

$$\frac{u_\infty}{u_{s\infty}} = \frac{1}{\beta}\sqrt{\frac{C_{s\infty}}{C_\infty}} \qquad (11)$$

Since, as mentioned earlier, in the region of turbulent flow the drag coefficient depends only on the particle shape, and since β is always a factor characteristic of the shape, Equation (11) is an expression of the fact that the terminal velocity of a fluid particle can be obtained from that of the equivalent sphere simply by applying a factor which is a function solely of the particle shape; that is,

$$\frac{u_\infty}{u_{s\infty}} = \phi_1\,(\text{shape}) \qquad (12)$$

[The existence of this correlation was touched upon by the author in a previous paper (*20*).]

In Appendix 1 it is proved, on the other hand, that the shape of a fluid particle depends only on a dimensionless group, called hereafter *Eötvös number.* Thus combining Equation (12) and Equation (41) of Appendix 1 gives

$$\frac{u_\infty}{u_{s\infty}} = \phi_2(N_{E\ddot{o}}) \qquad (13)$$

and from Equations (10) and (13)

$$\frac{C^*_\infty}{C_{s\infty}} = \left[\frac{1}{\phi_2\,(N_{E\ddot{o}})}\right]^2 = \phi_3\,(N_{E\ddot{o}}) \qquad (14)$$

It should be noticed however that the derivation of Equation (41) of Appendix 1 has been based on a fairly simplified model. Thus (1) the effect of finite viscosity of the particles has been neglected. This may affect the result both in case of small Eötvös numbers, because the circulation inside the particles is known to depend on the viscosity of particle (*5, 17, 41*) and because the circulation has been found to reduce the viscous shear, which in this region contributes in a larger percentage to the total drag, and in case of large Eötvös numbers, because the increasing particle viscosity exerts an increasing damping on the shape oscillation and in this way reduces the form drag; and (2) the zigzagging or spiraling of the particles which results in an apparent increase of the drag coefficient has also been disregarded. It will be seen later that these side motions of the particles are caused by a wake reaction and thus are dependent on the velocity and other factors influencing the shape of the wake.

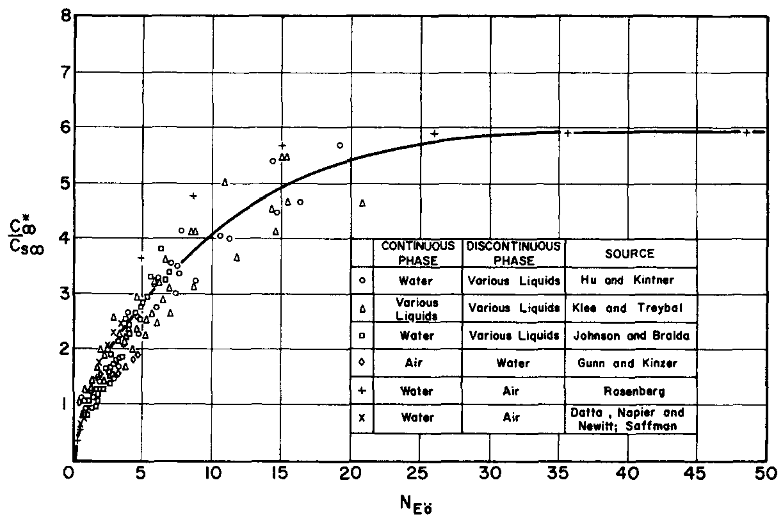

Fig. 1. Variation of drag coefficient with Eötvös number.

Neglecting these factors has undoubtedly been responsible for the fact that, as will be seen, a $u_\infty/u_{s\infty}$ vs. $N_{E\ddot{o}}$ correlation established for liquid or gas particles moving in liquid media is only a rough approximation if applied to liquid droplets falling in gaseous media.

An experimental proof of the validity of Equation (14) for liquid-liquid systems was given by Licht and Narasimhamurty (*31*), who found that for lower Eötvös numbers the $C^*_\infty/C_{s\infty}$ vs. $N_{E\ddot{o}}$ correlation can be approximated by a straight line. For gas-liquid systems Haberman and Morton (*16*) yielded an indirect proof by plotting C^*_∞ against the Weber number and showing that the curves representing widely different systems can thus be brought close together. In Appendix 1 it has been pointed out that in the turbulent region the Eötvös and the Weber numbers are equivalent as variables.

A fairly rapid variation of the $C^*_\infty/C_{s\infty}$ ratio is expected in the region of ellipsoidal particle shapes where, as observations show, the proportions of the particles vary markedly with size, that is with the Eötvös number. On the other hand, the dimension ratios of a spherical cap-shaped particle are practically independent of size (*9, 40*); therefore for large Eötvös numbers the $C^*_\infty/C_{s\infty}$ ratio is expected to become constant.

Experimental data of several authors have been used to plot the $C^*_\infty/C_{s\infty}$ ratio against the Eötvös number in Figure 1. Although the spread of the points is considerable, the expected tendency for variation of the $C^*_\infty/C_{s\infty}$ ratio with the Eötvös number is obvious. $C^*_\infty/C_{s\infty}$ values less than unity at very low Eötvös numbers indicate the effect of internal circulation. At higher Eötvös numbers the points for air bubbles are somewhat higher than those for liquid drops, probably because of the lack of damping effect of particle viscosity on shape oscillation.

Hu and Kintner (*23*) derived a correlation which, according to this terminology, states that liquid particles moving in liquid or gaseous media are not stable and will split up if $N_{E\ddot{o}} > 14.2$. Based on Keith and Hixson's (*26*) estimations for liquid-liquid systems the disintegration takes place in the range $7 < N_{E\ddot{o}} < 13$. For liquid particles falling through air Merrington and Richardson (*33*) have found the range of splitting up to be $8 < N_{E\ddot{o}} < 25$. So far there seems to be fair agreement between the observations. The agreement suddenly vanishes however if one completes this brief survey of fluid particle stability with the case of gas bubbles rising in liquids. On the basis of the experimental results of Rosenberg (*40*) and Haberman and Morton (*16*) one may even assume that bubbles with Eötvös numbers as high as 450 can still be regarded as stable. Apparently the Eötvös number alone does not provide a satisfactory stability criterion. Nevertheless it seems proba-

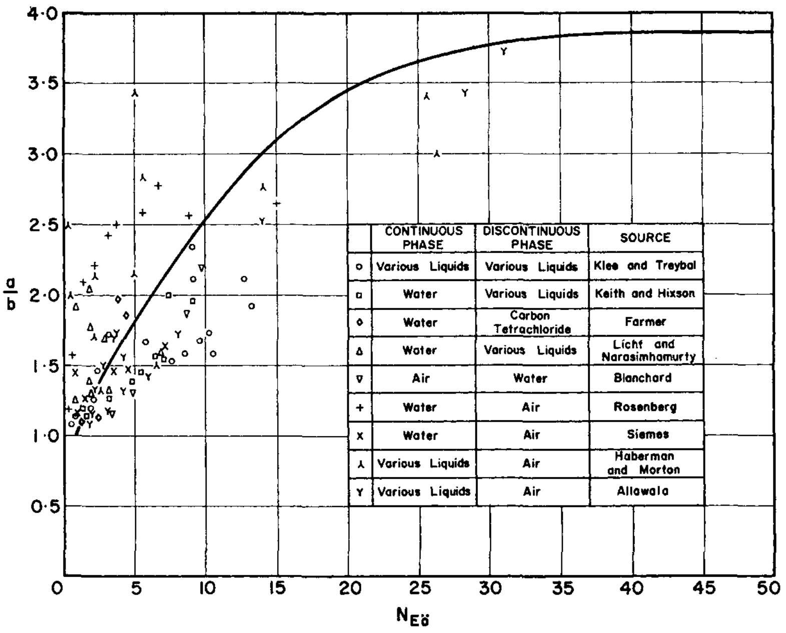

Fig. 2. Variation of particle shape with Eötvös number.

ble that the liquid drops never reach the region of spherical cap shape, which begins approximately at $N_{Eö} = 40$. In fact no point representing liquid particles can be found in Figure 1 above $N_{Eö} = 21$.

The spread of the points in Figure 1 cannot be attributed simply to the disregarded factors. There are strong signs that in some instances erroneous interfacial-tension determinations account for the discrepancies. In cases where the spread of points in noticeable, like the case seen in Figure 1, the best correlation of the points is the simplest one. In the range $N_{Eö} < 13$, which roughly corresponds to the region of moderately distorted ellipsoidal shapes, the approximation of

$$\frac{C^*_\infty}{C_{s\infty}} = 1.29\, N_{Eö}^{1/2} \quad (N_{Eö} < 13) \tag{15}$$

offers certain practical advantages. By combining it with Equation (10) one obtains

$$\frac{u_\infty}{u_{s\infty}} = \frac{0.88}{N_{Eö}^{1/4}} \tag{16}$$

which, after substitution for $u_{s\infty}$ from Equation (7) with $K_{s\infty} = 1.74$, becomes

$$u_\infty = 1.53 \left(\frac{g\, \Delta\rho\, \sigma}{\rho_c^2} \right)^{1/4} \tag{17}$$

It is seen that if one takes the $C^*_\infty/C_{s\infty}$ ratio proportional to the square root of the Eötvös number, the particle diameter is eliminated from the expression of terminal velocity.

The fact that under turbulent flow conditions the terminal velocity of liquid particles moving in liquid media is practically independent of the particle size is well known from various publications (*23, 26, 27*). The velocity of gaseous particles rising in liquid media seems to be somewhat more dependent on the particle size; however Equation (17) still yields satisfactory predictions if not applied to very small ($N_{Eö} < 1$) bubbles. The failure of Equation (17) in the region of very low Eötvös numbers is obviously a result of disregarding the effect of particle viscosity on the terminal velocity.

In the case of liquid particles falling through gaseous media the accuracy of Equation (17) is generally very poor. The velocity increases with the particle size throughout the whole region of turbulent flow, and although Equation (17) gives a fairly good prediction for the middle of the region, the deviation between the measured and calculated values may be as high as 25% toward the ends. This discrepancy is not surprising if one considers the markedly different characteristics of this system and the average of fifty times higher values of the terminal velocity.

It is interesting to note that Peebles and Garber (*36*) derived a correlation similar to Equation (17) for the spherical cap-shaped bubbles. It was undoubtedly a significant wall effect which caused them to reach that result. It will be pointed out later that for very large bubbles the terminal velocity depends on the tube diameter rather than on the bubble size, even if the d/D ratio is as low as 0.3.

From Equation (16) $u_\infty \to \infty$ if $N_{Eö} \to 0$; therefore it might be thought that the applicability of this equation should be limited toward low Eötvös numbers. With liquid-liquid systems such limitation is not necessary, since it is remembered that none of the given correlations can be used if $N_{Re} < 500$, and in this way a lower limit is automatically imposed on the Eötvös numbers (approximately $N_{Eö} = 0.7$). In the case of gas bubbles however the use of Equations (16) and (17) is not recommended for Eötvös numbers lower than 1.0.

It has been mentioned that in the region of spherical cap-shaped particles ($N_{Eö} > 40$) the shape is independent of the particle size; therefore as expected, the $C^*_\infty/C_{s\infty}$ ratio is a constant (see Figure 1.) On the basis of the measurements of Rosenberg (*40*) and

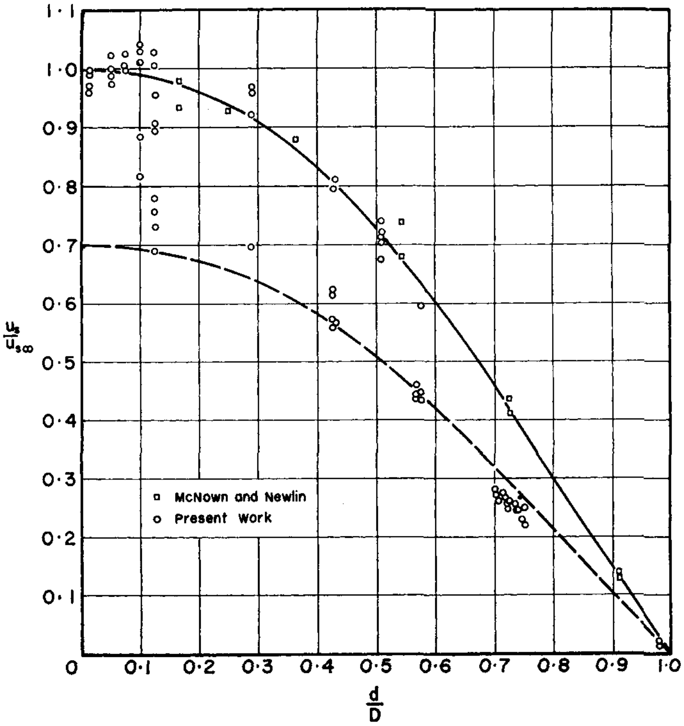

Fig. 3. Velocity of falling spheres in restricted media.

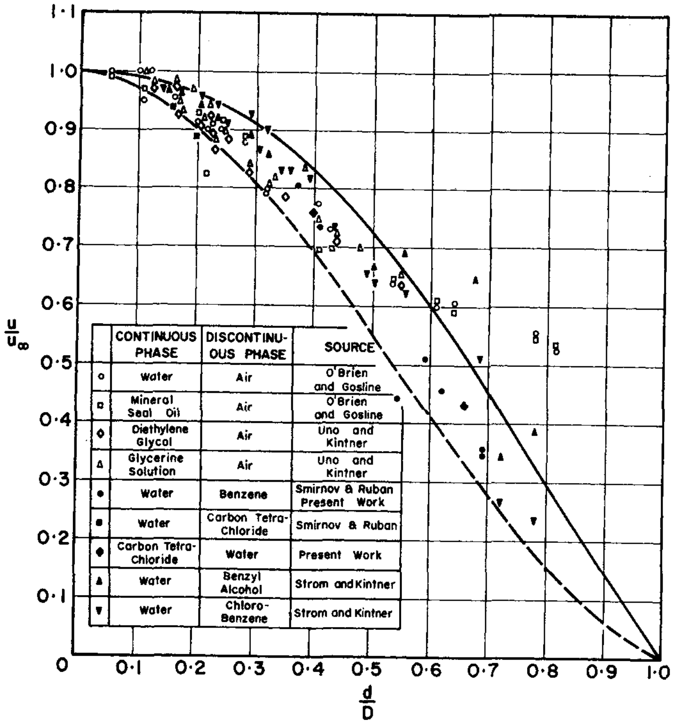

Fig. 4. Velocity of fluid particles in restricted media.

Haberman and Morton (*16*) the value of the constant is 2.6/0.44 = 5.91, which is reached after a fairly long transitional region ($13 < N_{Eo} < 40$) in which the variation of $C^*_\infty/C_{s\infty}$ is very slow.

Applying Equation (10) for the region of spherical cap-shaped particles, one gets

$$\frac{u_\infty}{u_{s\infty}} = 0.411 \quad (N_{Eo} > 40) \qquad (18)$$

in agreement with the observations of several research workers (*9, 16, 38, 40*).

SHAPE OF FLUID PARTICLES

If one accepts the general practice of characterizing the shape of a fluid particle by the ratio of the horizontal diameter to the vertical length, then as an alternative form for Equation (41) of Appendix 1 one can write

$$\frac{a}{b} = \phi_4\,(N_{Eo}) \qquad (19)$$

However if one tries to use the data reported in the literature (*1, 2, 12, 16, 26, 27, 31, 40, 45*) to plot a/b against the Eötvös number, a mass of widely scattered points will result, as shown in Figure 2. This enormous spread is undoubtedly due to shape oscillation, which, as the photographs taken by Licht and Narasimhamurty (*31*) show, may cause the a/b ratio for a given particle size to vary in a range with an upper limit three times as large as the lower limit. Under such conditions a multitude of photographs are required to determine the true average shape.

There is however another way of finding the explicit form of Equation (19). The wind-tunnel measurements of Riabouchinsky (*24, 39*) show that in the fully turbulent range of flow the drag coefficient of an oblate spheroid can be expressed in the following form:

$$\frac{C_{E\infty}}{C_{s\infty}} = 1 + \left(1 - \frac{b}{a}\right)\left(\frac{C_{P\infty}}{C_{s\infty}} - 1\right) \qquad (20)$$

Owing to the spiraling, zigzagging motion, shape oscillation, and deviations from the true spheroidal form, the drag coefficient of a fluid particle will be expressed as

$$C_\infty = \epsilon C_{E\infty} \qquad (21)$$

By combining Equations (4), (20), and (21) and substituting $C_{s\infty} = 0.44$ and $C_{P\infty} = 1.10$, one obtains

$$\frac{C^*_\infty}{C_{s\infty}} = \epsilon\beta^2\left(2.5 - 1.5\frac{b}{a}\right) \qquad (22)$$

Figure 2 is a graphical representation of this equation. It has been based on the $C^*_\infty/C_{s\infty}$ vs. N_{Eo} correlation shown in Figure 1 and the following assumptions:

1. Up to $N_{Eo} = 15$ the fluid particle is spheroidal [that is, β is substituted from Equation (5)] and ϵ is independent of N_{Eo} and equals 1.15.
2. Above $N_{Eo} = 40$ the particle is spherical cap shaped [that is, Equation (6) describes the correlation between β and a/b], and since the motion is practically rectilinear, $\epsilon = 1.0$.
3. In the range $15 < N_{Eo} < 40$ the shape gradually changes from spheroid to spherical cap and ϵ from 1.15 to 1.0.

It is seen that for the spherical-cap region $a/b = 3.85$, in good agreement with Rosenberg's experimental value 4.02 (*40*).

EFFECT OF WALL PROXIMITY

Since in practice the extent of the continuous medium around the moving fluid particle is always more or less restricted, it is extremely important to know the effect of the wall proximity on the particle. In fact a new variable enters the problem of particle motion—the diameter (or equivalent diameter) of the container D. This will result in the appearance of a new dimensionless variable in Equation (13), and according to the basic theorem of the dimensional analysis this new variable is d/D. The more complete form of Equation (13) is therefore

$$\frac{u}{u_{s\infty}} = \phi\left(N_{Eo}, \frac{d}{D}\right) \qquad (23)$$

Since the particles for which $N_{Eo} \to 0$ behave like solid spheres, it seemed reasonable to start the investigation by studying the effect of cylindrical wall on the motion of solid spheres.

Several publications deal with the velocity (or drag)) of spheres moving (or suspended) in the axis of a cylindrical channel under turbulent flow conditions (*10, 18, 34, 49*). In practice however the spheres rarely move along the axis of the cylinder; therefore the author thought it necessary to carry out a few experiments with spheres falling freely in tubes filled with different liquids.

TABLE 1. DIAMETER AND DENSITY OF SPHERES AND LIQUID COLUMNS USED

Spheres								Liquid columns			
No.	Material	d, cm.	ρ_D, g./cc.	No.	Material	d, cm.	ρ_D, g./cc.	No.	Material	D, cm.	ρ_C, g./cc.
1	Plastic 1	1.571	1.049	8	Plastic 2	0.931	1.167	1	Methanol	2.184	0.789
2	Plastic 1	1.565	1.053	9	Plastic 2	0.934	1.170	2	Carbon tetrachloride	2.202	1.590
3	Plastic 2	1.534	1.184	10	Plastic 2	0.929	1.172	3	Water	2.174	0.998
4	Plastic 2	1.249	1.171	11	Plastic 2	0.937	1.172	4	Methanol	1.264	0.789
5	Plastic 2	1.240	1.169	12	Glass	0.634	2.283	5	Carbon tetrachloride	1.248	1.590
6	Plastic 2	1.234	1.176	13	Glass	0.158	2.283	6	Water	1.243	0.998
7	Plastic 2	0.935	1.162	14	Steel Alloy	0.635	7.948	7	Water	12.40	0.998

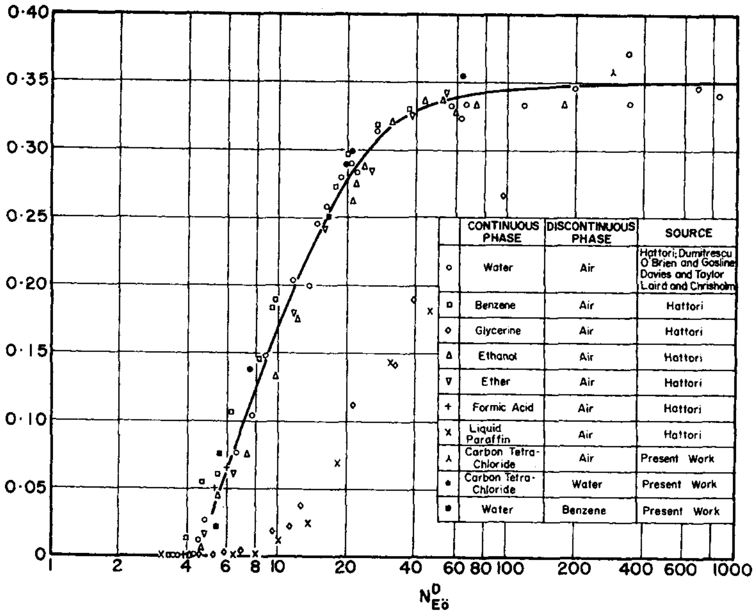

Fig. 5. Velocity coefficient of cylindrical particles.

Table 1 contains information about the diameter of spheres and tubes and the density of the spheres and liquids used in the experiments. In most cases the beads of a necklace of unknown plastic materials (denoted as plastic 1 and plastic 2) were used for spheres because of their convenient density and very good sphericity. The hole in them was partly filled with cement, accounting for the small spread in their density.

The time of fall of the spheres was measured on a 90- or 100-cm. distance with a stop watch. It was assumed that after 30 cm. of fall the spheres closely approached their terminal velocities. The measured velocities ranged from 0.94 cm./sec. to 83.4 cm./sec.

Points calculated from the experimental results of the author are plotted in Figure 3. A few other points, determined from the drag coefficient measurements of McNown and Newlin (*34*) for the range $7{,}000 < N_{Re} < 20{,}000$, are also shown. It is seen that part of the points, those representing the spheres falling in rectilinear or very steep helical paths, closely follow a curve, the equation of which is

$$\frac{u_s}{u_{s\infty}} = \frac{1-\left(\frac{d}{D}\right)^2}{\sqrt{1+\left(\frac{d}{D}\right)^4}} \qquad (24)$$

or for $\frac{d}{D} < 0.5$

$$\frac{u_s}{u_{s\infty}} \approx 1-\left(\frac{d}{D}\right)^2 \left(\frac{d}{D} < 0.5\right) \qquad (25)$$

Equation (24) was developed in a semiempirical way in Appendix 3*. Many other correlations were also examined, but none of them could follow the course of those points satisfactorily in the whole $0 < d/D < 1$ interval.

A considerable number of the points, representing the badly oscillating, zigzagging spheres or those not oscillating but rolling down on the tube wall, are located along a curve passing about 30% lower (see the dotted curve of Figure 3) than the curve of Equation (24). At large d/D ratios the zigzagging spheres frequently knocked against the tube wall; probably this fact accounts for the additional velocity drop at large d/D values.

Some spheres started as zigzagging, but later their paths straightened out. Points pertaining to such cases lie between the above-mentioned two curves.

An investigation into the nature and causes of oscillation was beyond the scope of this work. However it did not require too much attention to realize that the strong zigzagging was caused by the reaction of the wake, disturbed by the proximity of wall, on the spheres. This reaction is obviously less for fast-moving spheres; therefore the intensity of oscillation is a function of the absolute velocity, as well as the d/D ratio.

No general rule on the behavior of spheres in the proximity of the wall can be given. Sometimes even the deliberately eccentrically released balls seemed to steer themselves after a few oscillations to the axis of the tube. In other instances the almost concentrically dropped spheres turned to the wall and rolled down on it throughout.

Theoretical considerations, empirical formulas (*18*), and observations (*48, 49*) equally support the view that in the region concerned the terminal velocity reduction caused by the wall effect is practically independent of the shape of the particle if the a/D ratio is used instead of d/D. If one combines this fact with the observation that increasing d/D ratio increases the deformation of fluid particles, as well as the tendency of zigzagging, and thus decreases the u/u_∞ ratio beyond that predicted by Equation (24), then one can make a rough estimation of the velocity of fluid particles in media of restricted extent.

In Figure 4 the variation of the terminal velocity of fluid particles can be seen with increasing d/D ratio. The majority of the points represent data taken from the literature (*35, 46, 48, 49*). A few other points have been located on the basis of the author's measurements. Systems 2, 3, 5, 7, and 8 of Table 2 were used in the experiments. The values of the surface or interfacial tension have been taken from the literature (*19, 37*).

The particle diameter was calculated either from the volume measured in a capillary tube before release or, in case of droplets issued under quasistatic conditions, from the orifice diameter by means of Equation (43) of

* Appendix 3 has been deposited as document 6265 with the American Documentation Institute, Photoduplication Service, Library of Congress, Washington 25, D. C., and may be obtained for \$1.25 for photoprints or for 35-mm. microfilm.

TABLE 2. SYSTEMS USED FOR STUDYING WALL EFFECT AND CYLINDRICAL PARTICLE VELOCITY

No.	Continuous phase	Discontinuous phase	D, cm.	ρ_C, g./cc.	ρ_D, g./cc.	σ, dynes/cm.
1	Carbon tetrachloride	Water	2.202	1.590	0.998	45.0
2	Carbon tetrachloride	Water	2.184	1.590	0.998	45.0
3	Carbon tetrachloride	Water	1.264	1.590	0.998	45.0
4	Carbon tetrachloride	Water	1.248	1.590	0.998	45.0
5	Carbon tetrachloride	Water	0.765	1.590	0.998	45.0
6	Carbon tetrachloride	Air	2.202	1.590	0.001	26.3
7	Water	Benzene	2.184	0.998	0.877	35.0
8	Water	Benzene	1.264	0.998	0.877	35.0
9	Water	Benzene	1.248	0.998	0.877	35.0

Appendix 2. Two orifices were used, one of 0.353 and the other of 0.487-cm. diameter.

Whenever available, experimentally determined values of u_∞ (*16, 48, 49*) were used for calculating the u/u_∞ ratio. In the rest of the cases u_∞ was computed by means of Equation (17).

It is seen that up to about $d/D \approx 0.45$ the majority of the points in Figure 4 lie somewhat below the curve representing Equation (24) developed for solid spheres. The decrease of velocity due to the increased zigzagging tendency in restricted media is apparently much less for fluid particles than it was for solid spheres. The explanation is probably that in the turbulent range of spheroidal shapes the fluid particles always keep spiraling or zigzagging, even if $d/D = 0$, but the solid spheres move smoothly enough in infinite media.

The plotted points correspond to a size range of $0.31 < d < 4.45$ cm. and an Eötvös number range of $0.75 < N_{Eo} < 519$. Because of the considerable spread of the points the apparently slight effect of the Eötvös number on the u/u_∞ ratio cannot be detected from the figure. From the quality of the correlation found by Uno and Kintner (*49*) between u/u_∞ and σ on the one hand and u/u_∞ and D on the other, one can conclude however that u/u_∞ does in fact depend on the Eötvös number. On the basis of a study of their observations, and of the location of points in Figure 4, it seems to be a very plausible assumption that the lower the Eötvös number the nearer the u/u_∞ vs. d/D curve passes to that of the solid spheres. This fact is expressed in the following empirical equation:

$$\frac{u}{u_\infty} = \frac{1-\left(\frac{d}{D}\right)^2}{\sqrt{1+\left(\frac{d}{D}\right)^4}} \times \left[1-\frac{2}{3}\frac{N_{Eo}}{1+N_{Eo}}\left(\frac{d}{D}\right)^{3/2}\right] \qquad (26)$$

The curve pertaining to Eötvös numbers approaching infinity is also shown in Figure 4 as a dotted line.

Combining Equations (16) and (26) yields an explicit form for Equation (23):

$$\frac{u}{u_{s\infty}} = \frac{0.88}{N_{Eo}^{1/4}}\frac{1-\left(\frac{d}{D}\right)^2}{\sqrt{1+\left(\frac{d}{D}\right)^4}} \times \left[1-\frac{2}{3}\frac{N_{Eo}}{1+N_{Eo}}\left(\frac{d}{D}\right)^{3/2}\right] \qquad (27)$$

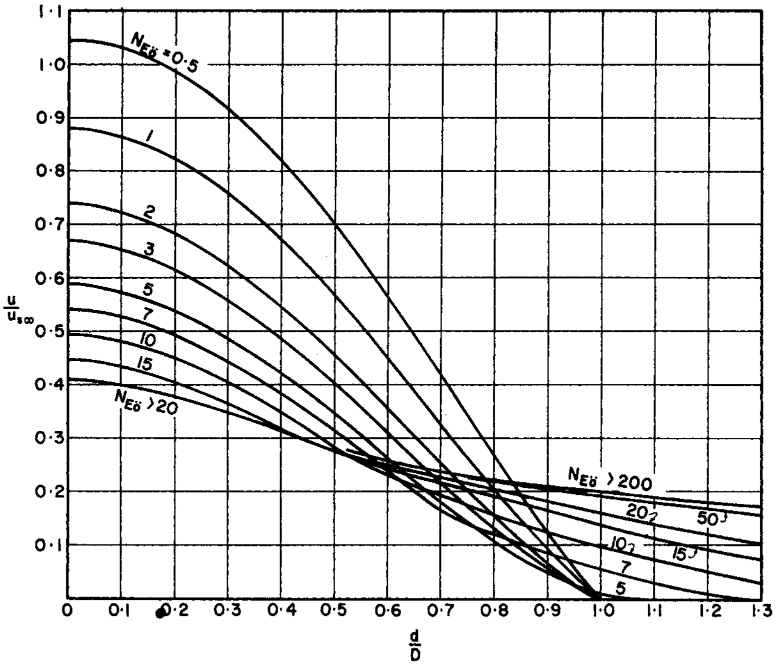

Fig. 6. Generalized chart for calculating the velocity of fluid particles.

which is applicable whenever

$$\frac{d}{D} < 1.0 \quad \text{for } N_{Eo} \leqq 4.5$$

$$\frac{d}{D} < 1 - 0.175\sqrt{N_{Eo} - 4.5} \quad \text{for } 4.5 < N_{Eo} < 20$$

$$\frac{d}{D} < 0.31 \quad \text{for } N_{Eo} \geqq 20 \qquad (28)$$

From Figure 4 it can be observed that above $d/D = 0.45$ the spread of the points becomes more and more noticeable because part of the particles assume velocities which are no longer dependent on their size but on the tube diameter.

CYLINDRICAL BUBBLES AND DROPS

A number of papers (*9, 11, 21, 28, 35*) concerned with the description and velocity of cylindrical bubbles have been published. The general conclusion is that the velocity of cylindri-

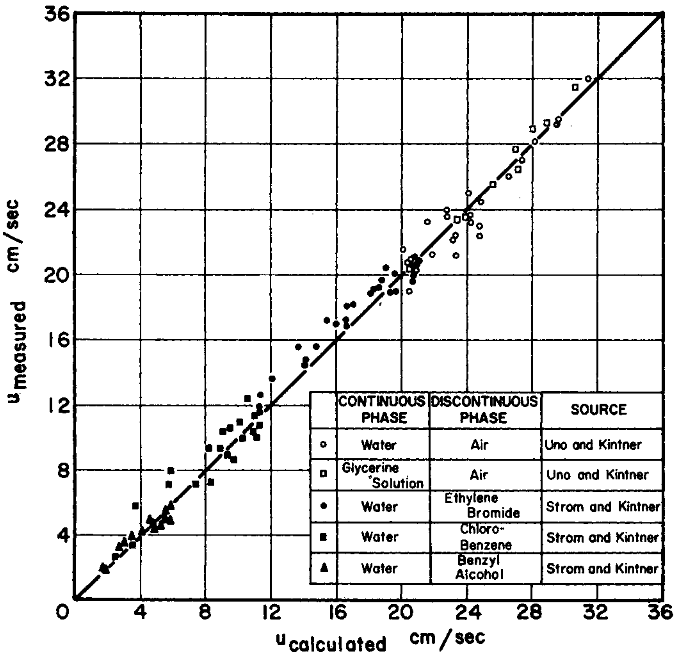

Fig. 7. Comparison of measured and calculated velocities.

cal bubbles is practically independent of the bubble volume and can be expressed as

$$u = \lambda \sqrt{\frac{g \Delta\rho D}{\rho_c}} \tag{29}$$

where λ has been recognized by Dumitrescu (*11*) as being a function of the $D\sqrt{g\Delta\rho/\sigma}$ group [which in this notation is identical with $(N^D{}_{Eo})^{1/2}$].

To study the variation of λ, the experimental data of the above-mentioned authors have been used to plot λ against $N^D{}_{Eo}$ in Figure 5. A few points representing average values of the writer's measurements with cylindrical drops (so far not studied) and bubbles are also plotted. The systems used in these experiments are those denoted by numbers 1, 3, 4, 5, 6, 7, 8, and 9 in Table 2.

The majority of the points follow a definite course, regardless of whether they represent gas bubbles or liquid drops. The best curve through these points seems to have a horizontal asymptote of $\lambda = 0.35$.

The points of two systems with continuous phases of very high viscosity are located on a different curve which would probably approach the same asymptote. It seems therefore that $N^D{}_{Eo}$ is not the only variable on which λ depends; the other variable (or variables) however plays no significant part if the viscosity of the continuous phase is in the common range. The motion of cylindrical fluid particles in very viscous continuous phase will not be discussed further here.

Hattori (*21*) has defined a critical tube diameter (corresponding to $N^D{}_{Eo} = 3.36$) below which the gas bubbles are no longer capable of moving in the tube filled with liquid. It is improbable that such a critical diameter can be found for liquid-liquid systems because of the higher tendency of the drops to wet the tube wall if the velocity is sufficiently low. Around $N^D{}_{Eo} \approx 5$ the reproducibility of the drop velocities becomes generally very poor.

If Equation (29) is rewritten in the form

$$\frac{u}{u_{\infty}} = \lambda \left(\frac{N_{Eo}}{\left(\frac{d}{D}\right)^2} \right) \frac{1}{1.74\sqrt{\frac{d}{D}}} \tag{30}$$

one has an explicit form of Equation (23) for the range of cylindrical fluid particles. Values taken from the continuous curve of Figure 5 can be used for λ in Equation (30), which is applicable if

$$\frac{d}{D} > 1 - 0.175\sqrt{N_{Eo} - 4.5} \quad \text{for } 4.5 < N_{Eo} < 20$$

$$\frac{d}{D} > 0.31 \quad \text{for } N_{Eo} \geqq 20 \tag{31}$$

An interesting feature of Equation (30) is that, although it was derived for cylindrical fluid particles, in the case of large Eötvös numbers it holds good even in regions where the particles are far from being cylindrical.

Figure 6 is a graphical representation of Equations (27) and (30) over the appropriate intervals and offers a quick way for the determination of the velocity of fluid particles in liquids in the range $0 \leqq d/D \leqq 1.3$, which is most frequently met in practice. Again it should be emphasized that this graph must not be used below $N_{Re} = 500$, and in the case of gas bubbles it is not recommended for $N_{Eo} < 1$.

In Figure 7 the velocities calculated by the use of the above u/u_{∞} vs. d/D and N_{Eo} graph are compared with those measured by Strom and Kintner (*48*) and Uno and Kintner (*49*). The systems used in this plot are of widely different properties. The Eötvös number varies between 0.66 and 75, the d/D ratio between 0.01 and 0.78. The spread of the points is generally well within the limits of reproducibility of the measurements.

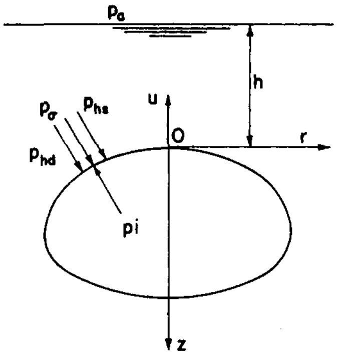

Fig. 8. Forces acting on surface of fluid particles.

ACKNOWLEDGMENT

The assistance of E. O. Porteous in the experiments is sincerely appreciated.

NOTATION

a = horizontal diameter of particle, cm.
A = $a^2\pi/4$, area of particle projected on a horizontal plane, sq.cm.
b = vertical size of particle, cm.
C = drag coefficient, dimensionless
d = spherical diameter, equivalent diameter of nonspherical particle, cm.
D = tube diameter, cm.
D_N = orifice diameter, cm.
F = drag, g.cm./sec.^{2} (= dyne)
g = acceleration due to gravity, 981 cm./sec.^{2}
h = distance from liquid surface, cm.
K = factor defined by Equations (8) and (9), dimensionless
N_{Eo} = $g\Delta\rho d^2/\sigma$, Eötvös number, dimensionless
$N^D{}_{Eo}$ = $g\Delta\rho D^2/\sigma$, Eötvös number referred to tube diameter, dimensionless
$N^{D_N}{}_{Eo}$ = $g\Delta\rho D_N{}^2/\sigma$, Eötvös number referred to orifice diameter, dimensionless
N_{Re} = $u_{\infty} d\rho_c/\mu$, Reynolds number, dimensionless
p = pressure, g./(cm.)(sec.^{2}) (= dynes/sq.cm.)
$\bar{p}$ = $p/\left(\rho_c \frac{u^2}{2}\right)$, dimensionless
r = variable (see Figure 8), cm.
$\bar{r}$ = r/d, dimensionless
R = curvature of particle surface, cm.
$\bar{R}$ = R/d, dimensionless
R_1, R_2 = principal curvatures of particle surface, cm.
$\bar{R}_1$, $\bar{R}_2$ = R_1/d, R_2/d, respectively, dimensionless
u = terminal velocity, cm./sec.
z = variable (see Figure 8), cm.
$\bar{z}$ = z/d, dimensionless

Greek Letters

α = latitude on the particle surface, dimensionless
β = factor defined by Equation (3), dimensionless, function of particle shape
ϵ = factor defined by Equation (21), dimensionless, function of Eötvös number
κ = factor defined by Equation (48), of Appendix 3, dimensionless
λ = factor defined by Equation (29), dimensionless
μ = viscosity, g./cm.sec (= poise)
ρ = density, g./cc.
$\Delta\rho$ = $|\rho_c - \rho_D|$, density difference, g./cc.
σ = surface tension or interfacial tension, g./sec.^{2} (= dynes/cm.)
ϕ, ϕ_1, ϕ_2, etc. = function

Subscripts

a = atmospheric
C = of continuous phase
D = of discontinuous phase
E = of oblate spheroid
hd = hydrodynamic
hs = hydrostatic
i = inside

O = at $z = 0$
P = of circular disk
s = of sphere
w = due to wall effect (in Appendix 3)
∞ = in infinite media
σ = due to surface or interfacial tension

Superscripts

$*$ = area of $d^2\pi/4$

LITERATURE CITED

1. Allawala, M. A., M.Sc. thesis, Illinois Inst. Technol., Chicago, (1952).
2. Blanchard, D. C., *Trans. Am. Geophys. Union*, **31**, 836 (1950).
3. Bond, W. N., *Phil. Mag.* (7), **4**, 889 (1927).
4. ———, and D. A. Newton, *ibid.*, **5**, 794 (1928).
5. Boussinesq, J., *Ann. Chim. Phys.*, **29**, 364 (1913).
6. Christiansen, R. M., *Dissertation Abstr.*, **15**, 1810 (1955).
7. Datta, R. L., D. H. Napier, and D. M. Newitt, *Trans. Inst. Chem. Engrs.* (*London*), **28**, 14 (1950).
8. Davies, C. N., *Proc. Phys. Soc.*, **51**, 259 (1945).
9. Davies, R. M., and Sir G. Taylor, *Proc. Roy. Soc.* (*London*), **A200**, 375 (1950).
10. Dubs, R., *Schweiz. Bauz.*, **97**, 169, 183 (1931).
11. Dumitrescu, D. T., *Z. angew. Math. u. Mech.*, **23**, 139 (1943).
12. Farmer, W. S., *U.S. Atomic Energy Comm.*, CRNL-635, Oak Ridge Natl. Lab. (1950).
13. Freud, B. B., and W. D. Harkins, *J. Phys. Chem.*, **33**, 1217 (1929).
14. Garner, F. H., *Trans. Inst. Chem. Engrs.* (*London*), **28**, 88 (1950).
15. Gunn, R., and G. D. Kinzer, *J. Meteorol.*, **6**, 243 (1949).
16. Haberman, W. L., and R. K. Morton, *The David W. Taylor Model Basin Report 802*, NS 715-102 (1953).
17. Hadamard, J., *Compt. rend. acad. sci. Paris*, **152**, 1735 (1911).
18. "Handbook of Aeronautics," Vol. I. p. 90, Sir Isaac Pitman & Sons Ltd., London, England (1938).
19. "Handbook of Chemistry and Physics," 35 ed., p. 1984, Chemical Rubber, Cleveland, Ohio (1954).
20. Harmathy, Tibor, *Acta. Tech. Acad. Sci. Hung.*, **12**, 209 (1955).
21. Hattori, S., *Rept. Aeronaut. Research Inst., Tokyo Imp. Univ.*, No. 115 (1935).
22. Hayworth, C. B., and R. E. Treybal, *Ind. Eng. Chem.*, **42**, 1174 (1950).
23. Hu, Shengen, and R. C. Kintner, *A.I.Ch.E. Journal*, **1**, 42 (1955).
24. Hughes, R. R., and E. R. Gilliland, *Chem. Eng. Progr.* **48**, 497 (1952).
25. Johnson, A. I., and L. Braida, *Can. J. Chem. Eng.*, **35**, 165 (1957).
26. Keith, F. W., and A. N. Hixson, *Ind. Eng. Chem.*, **47**, 258 (1955).
27. Klee, A. J., and R. E. Treybal, *A.I.Ch.E. Journal*, **2**, 444 (1956).
28. Laird, A. D. K., and D. Chrisholm, *Ind. Eng. Chem.*, **48**, 1361 (1956).
29. Laws, J. O., *Trans. Am. Geophys. Union*, Part III, p. 709, 22 Annual Meeting (1941).
30. Lewis, J. B., I. Jones, and H. R. C. Pratt, *Trans. Inst. Chem. Engrs.*, (*London*) **29**, 126 (1951).
31. Licht, William, and G. S. R. Narasimhamurty, *A.I.Ch.E. Journal*, **1**, 366 (1955).
32. Lohnstein, T., *Ann. Physik*, **20**, 237 (1906).
33. Merrington, A. C., and E. G. Richardson, *Proc. Phys. Soc.*, **59**, 1 (1947).
34. McNown, J. S., and J. T. Newlin, *Proc. First U.S. Natl. Cong. Appl. Mech.*, p. 801 (1951).
35. O'Brien, M. P., and J. E. Gosline, *Ind. Eng. Chem.*, **27**, 1436 (1935).
36. Peebles, R. N., and H. J. Garber, *Chem. Eng. Progr.*, **49**, 88 (1953).
37. Perry, J. H., "Chemical Engineers' Handbook," 3 ed., p. 363, McGraw-Hill, New York (1950).
38. Prandtl, L., "Essentials of Fluid Dynamics," p. 329. Hafner, New York (1952).
39. Riabouchinsky, D. P., *Aerodyn. Inst. Koutchino Bull.*, **5**, 73 (1921).
40. Rosenberg, B., *The David W. Taylor Model Basin Report 727*, (1950).
41. Rybczynski, W., *Bull. Acad. Sci. Cracovie*, **A**, 40 (1911).
42. Saffman, P. G., *J. Fluid Mech.*, **1**, 249 (1956).
43. Savic, P., *Natl. Res. Council* (*Canada*), Rept. No. MT-22 (1953).
44. Siemes, W., *Chem.-Ing.-Tech.*, **26**, 479 (1954).
45. *Ibid.*, 614 (1954).
46. Smirnov, N. I., and V. L. Ruban, *Zhur. Priklad. Khim.*, **22**, 1068 (1949).
47. *Ibid.*, **26**, 110 (1953).
48. Strom, J. R., and R. C. Kintner, *A.I.Ch.E. Journal*, **4**, 153 (1958).
49. Uno, Seiji, and R. C. Kintner, *ibid.*, **2**, 420 (1956).
50. Warshay, M., E. Bogusz, M. Johnson, and R. C. Kintner, *Can. J. Chem. Eng.*, **37**, 29 (1959).

Manuscript received March 25, 1959; revision received October 26, 1959; paper accepted October 29, 1959.

APPENDIX 1

The shape of fluid particles is determined by the forces acting along their surface. For the sake of simplicity a particle is examined which, when moving upward with its terminal velocity, is a body of revolution around the vertical axis, and its meridian curve is $r = r(z)$ (Figure 8).

The equilibrium of the forces is expressed by

$$p_i = p_{hs} + p_\sigma + p_{hd} \tag{32}$$

where

$$p_i = p_{io} + \rho_D gz \tag{33}$$

$$p_{hs} = p_a + \rho_c gh + \rho_c gz \tag{34}$$

$$p_\sigma = \sigma\left(\frac{1}{R_1} + \frac{1}{R_2}\right) \tag{35}$$

and under turbulent flow conditions

$$p_{hd} = \rho_c \frac{u^2}{2} \overline{p_{hd}}\,(\text{shape}, \alpha) \tag{36}$$

For $z = 0$, $R_1 = R_2 = R_0$, and $\overline{p_{hd}} = 1$; thus

$$p_{io} = p_a + \rho_c gh + \frac{2\sigma}{R_o} + \rho_c \frac{u^2}{2} \tag{37}$$

Combining Equations (32) to (37) one has

$$(\rho_c - \rho_D) gz + \sigma\left(\frac{1}{R_1} + \frac{1}{R_2} - \frac{2}{R_0}\right) - \rho_c \frac{u^2}{2}\left[1 - \overline{p_{hd}}(\text{shape}, \alpha)\right] = 0 \tag{38}$$

When one uses d as a characteristic length and the $\overline{r} = r/d$, $\overline{z} = z/d$, $\overline{R_0} = R_0/d$, $\overline{R_1} = R_1/d$, and $\overline{R_2} = R_2/d$ dimensionless quantities, the dimensionless form of Equation (38) becomes

$$\frac{g\Delta\rho d^2}{\sigma}\overline{z} + \frac{1}{\overline{R_1}} + \frac{1}{\overline{R_2}} - \frac{2}{\overline{R_0}} - \frac{1}{2}\frac{\rho_c d u^2}{\sigma} \times \left[1 - \overline{p_{hd}}(\text{shape}, \alpha)\right] = 0 \tag{39}$$

After one substitutes for $\overline{R_1}$ and $\overline{R_2}$ expressions in terms of $\overline{r}$ and $\overline{z}$, Equation (39) will be the one which, in principle, can be used for determining the $\overline{r} = \overline{r}(\overline{z})$ correlation, that is the shape of the fluid particle. But instead of getting into a hopelessly involved trial-and-error calculation, one should only draw the conclusion that in Equation (39) the following relationship is expressed:

$$\phi_5\left(\text{shape}, \frac{g\Delta\rho d^2}{\sigma}, \frac{\rho_c d u^2}{\sigma}\right) = 0 \tag{40}$$

Here the third group is the well-known Weber number. The second group can be recognized as a dimensionless form of the Laplace constant and plays an important part in such problems as the quasistatic bubble formation [see (*13*, *32*, *44*)], the formation of droplets among packing elements (*30*) or by breakup of jets (*6*), and the inception of internal circulation in liquid particles (*3*, *4*, *8*, *14*, *43*). It is suggested that this group be called *Eötvös number*.

A substitution for u from Equations (7) and (9) indicates however that in the turbulent region at a given particle shape and Eötvös number the Weber group does not impose an additional restriction on Equation (39), so that the shape of fluid particles moving in infinite media depends solely on the Eötvös group:

$$\text{shape} = \phi_6\,(N_{Eo}) \tag{41}$$

APPENDIX 2

On the basis of Siemes's study (*44*) on quasistatic bubble formation the following equation can be developed:

$$\frac{N_{Eo}^{\ 3}}{N^{DN}{}_{Eo}} = 21.6 \quad (42$$

or, if solved for d

$$d = 1.67\sqrt[3]{\frac{D_N\sigma}{\Delta\rho g}} \tag{43}$$

The validity of this equation for liquid-liquid systems can be proved by the application of Hayworth and Treybal's correlation (*22*) to very slowly forming droplets.